RESEARCH ARTICLE

GEOSCIENCES

Solar wind-magnetosphere energy influences the interannual variability of northern hemispheric winter climate

HE Shengping[1,2,3], WANG Huijun[2,3,4], LI Fei[5,2,4], LI Hui[6], and WANG Chi[6]

[1]Geophysical Institute, University of Bergen and Bjerknes Center for Climate Research, Bergen 5007, Norway;

[2]Key Laboratory of Meteorological Disaster/Collaborative Innovation Center on Forecast and Evaluation of Meteorological Disasters, Nanjing University of Information Science and Technology, Nanjing 210044, China;

[3]Climate Change Research Center, Chinese Academy of Sciences, Beijing 100029, China;

[4]Nansen-Zhu International Research Centre, Institute of Atmospheric Physics, Chinese Academy of Sciences, Beijing 100029, China;

[5]Norwegian Institute for Air Research, Kjeller 2007, Norway;

[6]State Key Laboratory of Space Weather, National Space Science Center, Chinese Academy of Sciences, Beijing 100190, China

Corresponding author. E-mail: Shengping.He@uib.no

Received December 16 2018; Revised April 8 2019; Accepted **

Abstract

Solar irradiance has been universally acknowledged to be dominant by quasi-decadal variability, which has been adopted frequently to investigate its effect on climate decadal variability. As one major terrestrial energy source, solar wind energy flux into the Earth's magnetosphere (E_{in}) exhibits dramatic interannual variation, the effect of which on Earth's climate, however, has not drawn much attention. Based on the E_{in} estimated by

three-dimensional magnetohydrodynamic simulations, we demonstrate a novelty that the annual mean E_{in} can explain up to 25% total interannual variance of northern hemispheric temperature in the subsequent boreal winter. The concurrent anomalous atmospheric circulation resembles the positive phase of Arctic Oscillation/North Atlantic Oscillation. The warm anomalies in the tropic stratopause and tropopause induced by increased solar wind-magnetosphere energy persist into the subsequent winter. Due to the dominant change in the polar vortex and mid-latitude westerly in boreal winter, a "top-down" propagation of the stationary planetary wave emerges in the Northern Hemisphere and further influence the atmospheric circulation and climate.

Keywords: solar wind, winter climate, interannual variability, stratosphere

Introduction

As the fundamental energy source of the earth's climate, the solar irradiance can dramatically influence the earth's climate, the earliest study of which can be traced back to the early eighteenth century [1]. It is well recognized that the variability of the solar activity (e.g. sunspot number, solar radio flux at 10.7 cm) exhibits mainly the quasi-decadal variability (i.e., prominent 11-year cycle) [2-4]. In the past over 100 years, there has been a growing body of evidence that the tropospheric and stratospheric climatic variables are affected by the solar activity in both global and regional scales [5-10].

In the stratosphere, the heating can be modulated by the solar cycle due to the variations of the ultraviolet absorption by ozone [11,12]. Associated with solar maximum, the upper stratospheric zonally averaged temperature at the equator, where the solar radiative input is the largest [13], is higher compared to that at solar minimum [14]. The increasing of solar radiative input during solar maximum can lead to 1–2°Cof increasing in the zonal-mean annual temperature located below the equatorial stratopause [15,16]. Such positive temperature anomalies intensify the mean poleward meridional temperature gradient and hence lead to anomalous westerly wind at mid-latitudes of the Northern Hemisphere [17,18]. As the propagation of the planetary waves has close relation to the background zonal winds, a downward propagation of atmospheric anomaly to mid- and high latitudes of lower stratosphere is generally observed at solar maximum [13,18,19]. Such a stratosphere 'top–down' influence provides a potential pathway in which the solar cycle influences the interdecadal variability of the tropospheric circulation and climate in the Northern Hemisphere.

It should be noted that most of the previous studies have adopted the parameters, that are dominated by quasi-decadal (i.e., 11-year cycle) variability, to investigate the solar impacts on the atmospheric circulation and climate. Such solar cycle- atmosphere/climate relationships are not a simple linear correlation on interannul time scale but, rather, a kind of decadal modulation effect of the 11-year solar cycle. For example, by comparing the solar maximum with the solar minimum periods, many studies have explored the different response of climate or investigated the different climatic impacts of other factors such as El Niño–Southern Oscillation (ENSO) [20,21], Arctic Oscillation [22,23], and North Atlantic Oscillation [24]. Actually, except for the quasi-decadal variability, higher frequency variability also exists in solar activity [25]. It is estimated that the energy of solar wind and cosmic rays can be increased by tens and hundreds times during solar maximum periods [26]. Therefore, it is very important to examine the potential influence of total energy input from the solar wind into the Earth's magnetosphere (E_{in}) on the interannual variability of climate, which is

rarely discussed before due to the big challenge in quantitatively estimation of E_{in} [27-29]. Utilizing the E_{in} quantitatively estimated by three-dimensional magnetohydrodynamics (see method section) [30], in this study, we reveal a novel influence of solar wind-magnetosphere energy on the winter climate over the Northern Hemisphere.

Solar wind-magnetosphere energy is linked to northern hemispheric winter temperature and atmospheric circulation

The sunspot number (SSN) shows apparent low-frequency variability with alternate positive and negative phases during which no apparent high-frequency variability is observed (Figure 1a). Even though alternate positive and negative phases are also observed in E_{in}, there are obvious high-frequency variability during positive/negative phases (Figure 1b). To illustrate clearly the time scale of the variability, we present, in Figures 1c and 1d, the spectral analysis on the time series. The results indicate that the SSN is dominated by decadal variability (Figure 1c) while the E_{in} displays both interannual and decadal variability (Figure 1d). Therefore, it's possible to investigate the interannual relationship between the E_{in} and the atmospheric circulation and climate.

[INSERT FIGURE 1 HERE].

Figure 2a indicates that, during the winters following higher E_{in} in the preceding year, significant warmer anomalies extend from northwest Europe through Siberia to northeast Asia and cross from Alaska to southwest Canada, with maximum amplitude of up to 0.9℃ over Eurasia. Meanwhile, significant colder anomalies emerge in south Europe (south of 45°N) and East Canada to the Greenland with the maximum amplitude of up to -0.8℃. The significant lag-relationship (with maximum correlation coefficients up to 0.5) indicates the possible forcing of solar wind-magnetosphere energy to the northern hemispheric winter climate. The results derived from GISTEMP Team [31] resembles those derived from NCEP/NCAR reanalysis (Figure 2b vs. 2a), with a spatial correlation of 0.78. It should be noted that the results will not show much difference when the linear influence of ENSO has been removed (not shown).

Boreal winter large-scale atmospheric circulation following higher-than-normal solar wind-magnetosphere energy is further explored. As shown in Figure 2c, corresponding to higher-than-normal annual mean E_{in}, the winters in subsequent year generally see significant positive sea level pressure (SLP) anomalies at mid-latitudes of the North Atlantic with the maximum anomaly of 2.4 hPa at the central Atlantic (around 45°N). The positive SLP anomalies extend across North America through the North Atlantic eastward to Eurasian

continent. At the same time, significant negative SLP anomalies are located in the Atlantic-Arctic sector with minimum values of −2.4 hPa centered at the Barents Sea. The spatial distribution of the winter SLP anomalies related to the higher-than-normal E_{in} in the preceding year resemble the positive phase North Atlantic oscillation (NAO) or Arctic Oscillation (AO) pattern. Similar NAO-/AO-like pattern is also found in the 500-hPa geopotential height anomalies (Figure 2d). Note that there is an additional significant positive anomaly center located over the Baikal, which is missing in the SLP field, indicating the possible "top-down" propagated influence of solar wind-magnetosphere energy. Results based on the interannual variability obtained from another filtering method [32] are similar (Figure S1). The spatial pattern of the temperature anomalies related to positive phase of AO/NAO (Figures S2a and S2c) resembles closely the one related to the higher-than-normal Ein (e.g., the spatial correlations of Figure 2a with Figures S2a and S2b are 0.81 and 0.86, respectively). It further supports speculation that the significant interannual relationship between the solar wind-magnetosphere energy and northern hemispheric winter climate may be attributed to the solar impacts on the NAO-/AO-related atmospheric circulation variability (Figure S3).

[INSERT FIGURE 2 HERE].

Stratospheric-tropospheric dynamical analyses

Following increasing of solar wind-magnetosphere energy, two statistically significant warming centers over tropical region (30°S−30°N) with magnitude of up to 0.5°C emerge in the upper troposphere (200−70 hPa ≈ 12−18 km) and stratopause, persisting from boreal spring (March to April) to boreal winter (Figures. 3a−3d; shading). The two warming responses might be caused by the increased solar ultraviolet irradiance and adiabatic warming as well as increased ozone heating [33,34]. In boreal winter, the higher solar wind-magnetosphere energy intensifies dramatically the stratospheric polar vortex [19] (Figure S4). Due to the intensification of the polar vortex, a dominant cooling of -0.9℃ emerges in the upper troposphere and lower stratosphere over the polar region (Figure 3d, shading). Consequently, the poleward temperature gradient is further intensified in boreal winter, which induces an apparent westerly wind anomaly at high latitudes with maximum acceleration in the speed of up to 1.8 m s^{-1} (around 60°N; Figure 3d, contours). Note that the interannual variability of zonal mean air temperature, high-latitude zonal wind, and polar vortex in boreal winter at lag +1 year responding to the E_{in} is in good agreement with the counterparts to the solar maximum revealed by Thiéblemont et al. [19]. It implies that the previously proposed pathway, on decadal time scale, can also link the solar activity to the

northern hemispheric climate on interannual time scale. Great potentials of impacts and applications could be explored from the solar wind-magnetosphere energy.

Anomalous zonal background flow can alter the planetary wave propagation from stratosphere downward to troposphere so as to connect the solar signals with the surface climate in boreal winter [35]. When there is higher annual mean solar wind-magnetosphere energy, the subsequent years' winters experience apparent anomalous E-P fluxes propagating from upper stratosphere downward into the troposphere at latitudes north of 60°N (Figure S5a: vectors). The anomalous downward propagations of the winter E-P flux may be induced by the acceleration of the high latitude westerly wind in winter (Fig. 3d: contours) which is unfavorable for the upward propagation of planetary waves [36]. The anomalous downward propagating planetary waves lead to E-P flux divergence anomalies in the stratosphere and upper troposphere at high latitudes (Figure S5: shading), which further accelerates the westerly wind and strengthens the polar vortex (Figure S4: shading) [35,37,38]. Such a mean flow-wave interaction in the stratosphere may provide one possible way to maintain the downward propagation of the solar signals [19]. It may be noted that apparent planetary waves propagate from the lower troposphere at mid-latitudes (between 30°−60°N) upwards upper troposphere (~ 100 hPa) and bend equator-ward (Figure S5: vectors), which may be induced by the mid-latitude sea surface temperature anomalies related to the solar wind-magnetosphere energy [19]. Because equatorward-pointing E-P fluxes correspond to poleward meridional eddy momentum flux, increasing of solar wind-magnetosphere energy induces eddy westerly momentum flux anomalies toward to the Arctic from middle to upper troposphere (Figure S5: vectors between 300−100 hPa). These poleward momentum fluxes further help to sustain anomalous westerly at high latitudes (north 60°N), causing downward migration of the westerly anomaly from stratosphere downward to troposphere so as to impact tropospheric circulation. Such mean flow-wave interaction in the troposphere favors the influence of solar wind-magnetosphere energy on the tropospheric circulation and climate.

[INSERT FIGURE 3 HERE].

The downward propagating winter atmospheric anomalies related to the solar wind-magnetosphere energy variability is very clear by inspecting the geopotential height anomalies. The geopotential height in subtropics of the North Atlantic, Eurasian continent, and North America shows significant increase anomalies from upper troposphere to stratosphere during spring, summer, and autumn (figures not shown). By the winter, the positive geopotential height anomalies propagate from the stratosphere downwards to lower troposphere at mid-latitudes (Figs. 4a−4c), which is most apparent over the North

Atlantic (Fig. 4a). The dominant downward propagating geopotential height anomalies at mid-latitudes in boreal winter may be related to the Brewer-Dobson circulation which is most active in boreal winter [39,40]. Concurrent with the changes in the geopotential height, significant westerly anomalies propagate from the stratosphere downwards to lower troposphere at high latitudes (around 60°N) (Figure S6a−S6c). Daily geopotential height anomalies also indicate that the significant positive height anomalies are located in the subtropical stratosphere before the end of November, which start to propagate downwards to troposphere in the end of November (Figure S7).

[INSERT FIGURE 4 HERE]

[INSERT FIGURE 5 HERE]

Consequently, two Rossby wave-like pattern are observed in the troposphere: one propagates from the North Pacific to North America and the other propagates from the North Atlantic eastward to Eurasia (Figures. S8a−S8c: vectors). The schematic is illustrated in Figure 5. The horizontal propagation of Rossby waves can influence the blocking frequency and therefore affect the winter climate over the Northern Hemisphere [41]. The frequency of winter Ural blocking is reduced significantly by over 30% corresponding to one standard deviation of increasing in the annual mean E_{in} in the preceding year (Figure S9a). As a results, the winter extreme cold (warm) days are significantly decreased (increased) over northern Eurasia (Figures. S9b−S9c). Meanwhile, the winter blocking frequency is increased by over 25% from North America to north Europe and decreased by over 35% from north Canada to the Greenland (Figure S9a). The significant anomalies of blocking frequency, extreme cold days, and extreme warm days in winter can explain well the anomalous winter climate over the Northern Hemisphere that are induced by the solar wind-magnetosphere energy variability.

Conclusions

Recent analyses of the solar/atmosphere relationship conducted by comparing two multi-decadal ocean-atmosphere chemistry-climate simulations with and without solar forcing variability revealed a significant response of boreal winter atmosphere at lag +1 year to the decadal variability (i.e., the 11-year solar cycle) [19]. However, the interannual relationship between the solar activity and the northern hemispheric climate has not drawn much attention.

Based on a new index estimated by three-dimensional magnetohydrodynamic simulations, this study reveals a novel statistically significant interannual relationship

between the annual mean E_{in} and the following boreal winter climate over the Northern Hemisphere. The high variance (up to 25%, i.e. r^2=0.25) of winter SAT over the Northern Hemisphere explained by preceding year's solar wind-magnetosphere energy sheds a promising improvement to climate predictions. It suggests that not only the quasi-decadal variability but also the interannual variability of solar activity should be taken account of in the climate prediction.

Data and method

Energy input from the solar wind into the Earth's magnetosphere (E_{in}) *and atmospheric variables*

The E_{in} (units: W) is estimated quantitatively by a three-dimensional magnetohydrodynamic simulation Wang et al. [30]:

$$E_{in} = 3.78\times10^{7} n_{SW}^{0.24} V_{SW}^{1.47} B_T^{0.86} [\sin^{2.70}\left(\frac{\vartheta}{2}\right) + 0.25].$$

Here, n_{SW} and V_{SW} are the solar wind number density (units: cm^{-3}) and solar wind velocity (units: km s^{-1}), respectively; B_T is the transverse magnetic field magnitude (units: nT), and ϑ is the interplanetary magnetic field clock angle. Solar wind data is obtained from OMNIweb (http://omniweb.gsfc.nasa.gov/) of Goddard Space Flight Center in National Aeronautics and Space Administration (NASA). Wang et al. [30] suggested that the E_{in} shows good performance in quantitatively estimating the energy input on the global scale.

Monthly mean and daily mean atmospheric variables are obtained from the National Centers for Environmental Prediction–National Center for Atmospheric Research (NCEP/NCAR) reanalysis [42]. Monthly mean surface temperature from Goddard Institute for Space Studies in NASA [31] is employed to support the results derived from NCEP/NCAR reanalysis.

Extreme events.

An extreme cold/warm day is define when a daily maximum temperature is lower (higher) than 10^{th} (90^{th}) percentile value [43]. The 10^{th} and 90^{th} percentile values are based on the daily maximum temperature during 1981−2010. Blocking high events are defined as intervals in which daily 500-hPa geopotential height from the NCEP/NCAR reanalysis exceeds one standard deviation above the monthly mean for each grid cell over five consecutive days [41,44].

Acknowledgements

This research was supported by the National Key R&D Program of China (2016YFA0600703) and the National Natural Science Foundation of China (Grants 41875118, 41505073 and 41605059).

Author contributions

S.H. designed the study. H.L. and C.W. provided the quantitatively estimation of the energy input from the solar wind into the Earth's magnetosphere. S.H. performed all the analysis and plotted the figures. S.H. wrote the initial manuscript, with input from H.W., F.L., H.L., and C.W.

Competing financial interests

The authors declare no competing financial interests.

References

1 Herschel, W. Observations tending to investigate the nature of the Sun, in order to find the causes or symptoms of its variable emission of light and heat; with remarks on the use that may possibly be drawn from solar observations. *Philosophical Transactions of the Royal Society of London* 1801; **91**: 265-318.

2 Willson, R. C. & Hudson, H. S. The Sun's luminosity over a complete solar cycle. *Nature* 1991; **351**: 42.

3 Camp, C. D. & Tung, K. K. Surface warming by the solar cycle as revealed by the composite mean difference projection. *Geophysical Research Letters* 2007; **34**.

4 Lean, J. Solar ultraviolet irradiance variations: A review. *Journal of Geophysical Research: Atmospheres* 1987; **92**: 839-868.

5 Labitzke, K. & Van Loon, H. Associations between the 11-year solar cycle, the QBO and the atmosphere. Part I: the troposphere and stratosphere in the northern hemisphere in winter. *Journal of Atmospheric and Terrestrial Physics* 1988; **50**: 197-206.

6 Loon, H. V. & Labitzke, K. Association between the 11-year solar cycle, the QBO, and the atmosphere. Part II: Surface and 700 mb in the Northern Hemisphere in winter. *Journal of Climate* 1988; **1**: 905-920.

7 Labitzke, K. & Van Loon, H. The signal of the 11-year sunspot cycle in the upper troposphere-lower stratosphere. *Space Science Reviews* 1997; **80**: 393-410.

8 Frederick, J. E., Tinsley, B. A. J. J. o. A. & Physics, S.-T. The response of longwave radiation at the South Pole to electrical and magnetic variations: Links to meteorological generators and the solar wind. 2018; **179**: 214-224.

9 Frederick, J. E. J. J. o. A. & Physics, S.-T. An analysis of couplings between solar activity and atmospheric opacity at the South Pole. 2017; **164**: 97-104.

10 Frederick, J. E. J. J. o. A. & Physics, S.-T. Solar irradiance observed at Summit, Greenland: Possible links to magnetic activity on short timescales. 2016; **147**: 59-70.

11 Gray, L. J., Rumbold, S. T. & Shine, K. P. Stratospheric temperature and radiative forcing response to 11-year solar cycle changes in irradiance and ozone. *Journal of the Atmospheric Sciences* 2009; **66**: 2402-2417.

12 Haigh, J. D. The role of stratospheric ozone in modulating the solar radiative forcing of climate. *Nature* 1994; **370**: 544.

13 Gray, L. J. *et al.* A lagged response to the 11 year solar cycle in observed winter Atlantic/European weather patterns. *Journal of Geophysical Research: Atmospheres* 2013; **118**.

14 Mitchell, D. *et al.* Signatures of naturally induced variability in the atmosphere using multiple reanalysis datasets. *Quarterly Journal of the Royal Meteorological Society* 2015; **141**: 2011-2031.

15 Crooks, S. A. & Gray, L. J. Characterization of the 11-year solar signal using a multiple regression analysis of the ERA-40 dataset. *Journal of Climate* 2005; **18**: 996-1015.

16 Frame, T. H. & Gray, L. J. The 11-yr solar cycle in ERA-40 data: An update to 2008. *Journal of Climate* 2010; **23**: 2213-2222.

17 Holton, J. R. in *Academic Press* (ed 3d ed.) (1992).

18 Gray, L. J. *et al.* Solar influences on climate. *Reviews of Geophysics* 2010; **48**.

19 Thiéblemont, R., Matthes, K., Omrani, N.-E., Kodera, K. & Hansen, F. Solar forcing synchronizes decadal North Atlantic climate variability. *Nature communications* 2015; **6**.

20 Calvo, N. & Marsh, D. R. The combined effects of ENSO and the 11 year solar cycle on the Northern Hemisphere polar stratosphere. *Journal of Geophysical Research: Atmospheres* 2011; **116**.

21 Zhou, Q., Chen, W. & Zhou, W. Solar cycle modulation of the ENSO impact on the winter climate of East Asia. *Journal of Geophysical Research: Atmospheres* 2013; **118**: 5111-5119.

22 Huth, R., Bochníček, J. & Hejda, P. The 11-year solar cycle affects the intensity and annularity of the Arctic Oscillation. *Journal of atmospheric and solar-terrestrial physics* 2007; **69**: 1095-1109.

23 Chen, W. & Zhou, Q. Modulation of the Arctic Oscillation and the East Asian winter climate relationships by the 11-year solar cycle. *Advances in Atmospheric Sciences* 2012; **29**: 217-226.

24 Kodera, K. & Kuroda, Y. A possible mechanism of solar modulation of the spatial structure of the North Atlantic Oscillation. *Journal of Geophysical Research: Atmospheres* 2005; **110**.

25 He, S.-P. *et al.* Influence of solar wind energy flux on the interannual variability of ENSO in the subsequent year. *Atmospheric and Oceanic Science Letters* 2018: 1-8.

26 Troshichev, O., Egorova, L., Janzhura, A. & Vovk, V. Influence of the disturbed solar wind on atmospheric processes in Antarctica and El-Nino Southern Oscillation (ENSO). *MEMORIE-SOCIETA ASTRONOMICA ITALIANA* 2005; **76**: 890.

27 Akasofu, S.-I. Energy coupling between the solar wind and the magnetosphere. *Space Science Reviews* 1981; **28**: 121-190.

28 Newell, P. T., Sotirelis, T., Liou, K. & Rich, F. Pairs of solar wind - magnetosphere coupling functions: Combining a merging term with a viscous term works best. *Journal of Geophysical Research: Space Physics* 2008; **113**.

29 HE, S.-P. *et al.* Influence of solar wind energy flux on the interannual variability of ENSO in the subsequent year. *Atmospheric and Oceanic Science Letters* 2018; **11**: 165-172.

30 Wang, C., Han, J., Li, H., Peng, Z. & Richardson, J. Solar wind - magnetosphere energy coupling function fitting: Results from a global MHD simulation. *Journal of Geophysical Research: Space Physics* 2014; **119**: 6199-6212.

31 GISTEMP Team. GISS surface temperature analysis (GISTEMP). *NASA Goddard Institute for Space Studies. Dataset accessed* 2016; **8**.

32 Sullivan, A. *et al.* Robust contribution of decadal anomalies to the frequency of central-Pacific El Niño. *Scientific reports* 2016; **6**: 38540.

33 Kodera, K. & Kuroda, Y. Dynamical response to the solar cycle. *Journal of Geophysical Research: Atmospheres* 2002; **107**.

34 Cionni, I. *et al.* Ozone database in support of CMIP5 simulations: results and corresponding radiative forcing. *Atmospheric Chemistry and Physics* 2011; **11**: 11267-11292.

35 Hartmann, D. L., Wallace, J. M., Limpasuvan, V., Thompson, D. W. & Holton, J. R. Can ozone depletion and global warming interact to produce rapid climate change? *Proceedings of the National Academy of Sciences* 2000; **97**: 1412-1417.

36 Charney, J. G. & Drazin, P. G. Propagation of planetary - scale disturbances from the lower into the upper atmosphere. *Journal of Geophysical Research* 1961; **66**: 83-109.

37 Andrewes, D. G., Holton, J. R. & Leovy, C. B. *Middle atmosphere dynamics*. (Academic press, 1987).

38 He, S., Wang, H., Gao, Y. & Li, F. Recent intensified impact of December Arctic Oscillation on subsequent January temperature in Eurasia and North Africa. *Climate Dynamics* 2018: 1-18.

39 Butchart, N. *et al.* Simulations of anthropogenic change in the strength of the Brewer–Dobson circulation. *Climate Dynamics* 2006; **27**: 727-741.

40 Weber, M. *et al.* The Brewer-Dobson circulation and total ozone from seasonal to decadal time scales. *Atmospheric Chemistry and Physics* 2011; **11**: 11221-11235.

41 Li, F., Orsolini, Y. J., Wang, H., Gao, Y. & He, S. Atlantic multidecadal oscillation modulates the impacts of Arctic sea ice decline. *Geophysical Research Letters* 2018; **45**: 2497-2506.

42 Kalnay, E. *et al.* The NCEP/NCAR 40-year reanalysis project. *Bulletin of the American Meteorological Society* 1996; **77**: 437-471. doi:10.1175/1520-0477(1996)077<0437:TNYRP>2.0.CO;2

43 He, S. & Wang, H. Linkage between the East Asian January temperature extremes and the preceding Arctic Oscillation. *International Journal of Climatology* 2016; **36**: 1026-1032.

44 Thompson, D. W. & Wallace, J. M. Regional climate impacts of the Northern Hemisphere annular mode. *Science* 2001; **293**: 85-89.

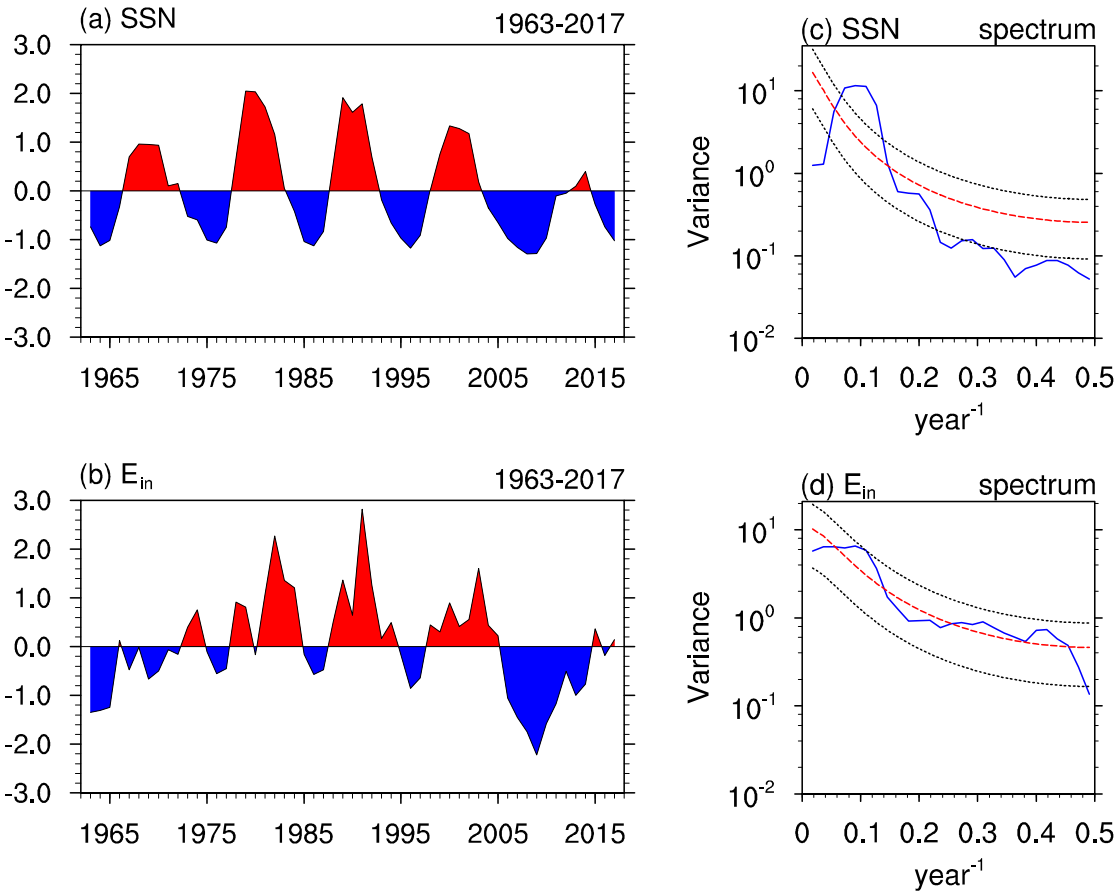

Figure 1. Decadal and interannual variability of solar variables. Normalized time series of annual mean (**a**) SSN, (**b**) E_{in} during 1963−2017. Spectral analysis (blue curves) for (**c**) SSN and (**d**) E_{in}, the red dashed line indicates the red noise confidence interval, the black dashed lines indicate the upper and lower confidence bounds.

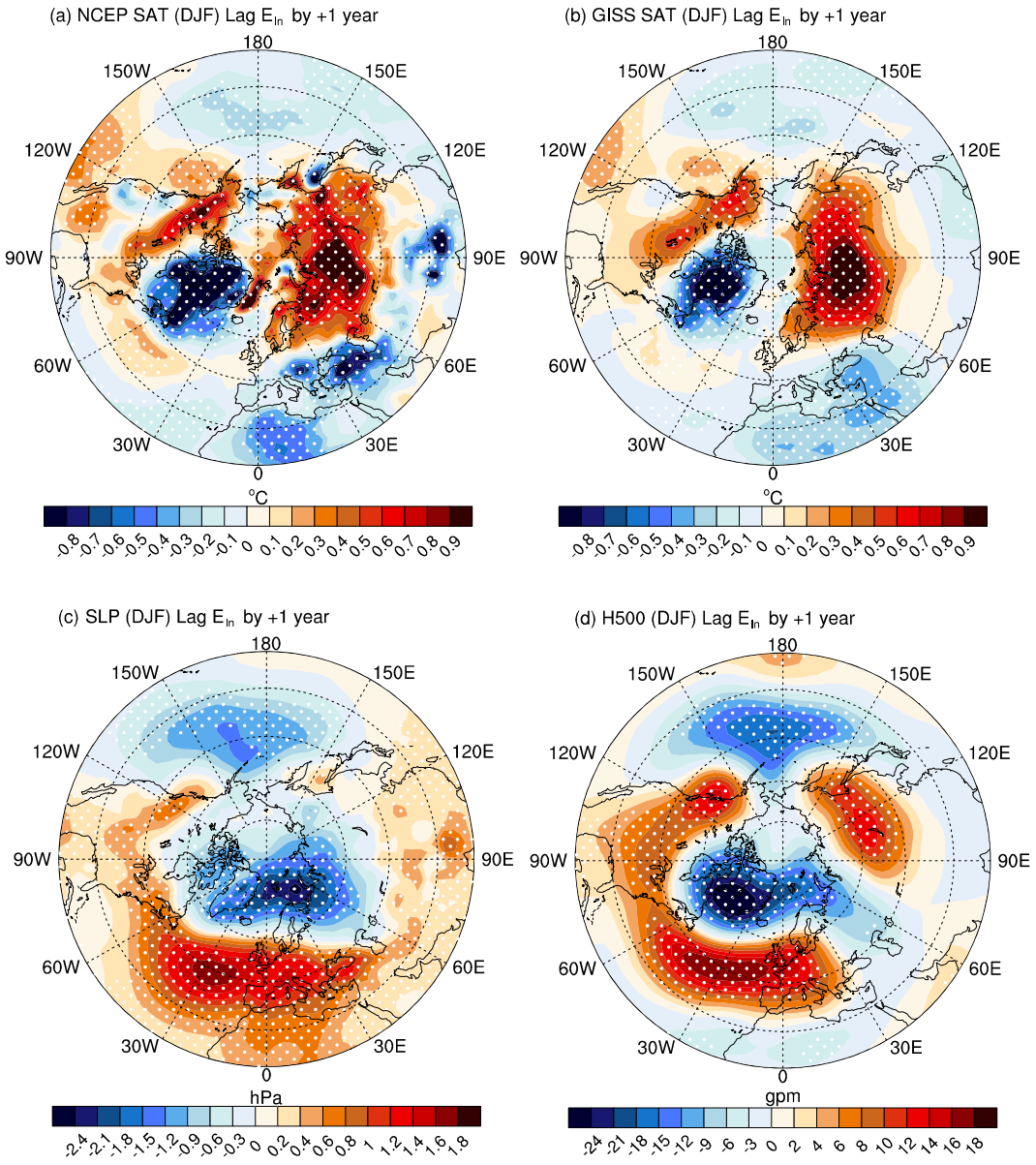

Figure 2. Lag relationship of boreal winter atmosphere with solar wind energy. (a) Regression maps of surface air temperature north of 20°N during winter (December, January, and February) 1964−2017 onto the normalized preceding annual mean of solar wind energy flux into the Earth's magnetosphere (E_{in}) index during 1963–2016. Surface air temperature derives from NCEP/NCAR reanalysis. Dotted values are significant at the 90% confidence levels. (b) same as (a), but the surface air temperature derives from National Aeronautics and Space Administration, Goddard Institute for Space Studies (http://data.giss.nasa.gov/gistemp/). (c) and (d) same as (a), but for the sea level pressure and 500-hPa geopotential height.

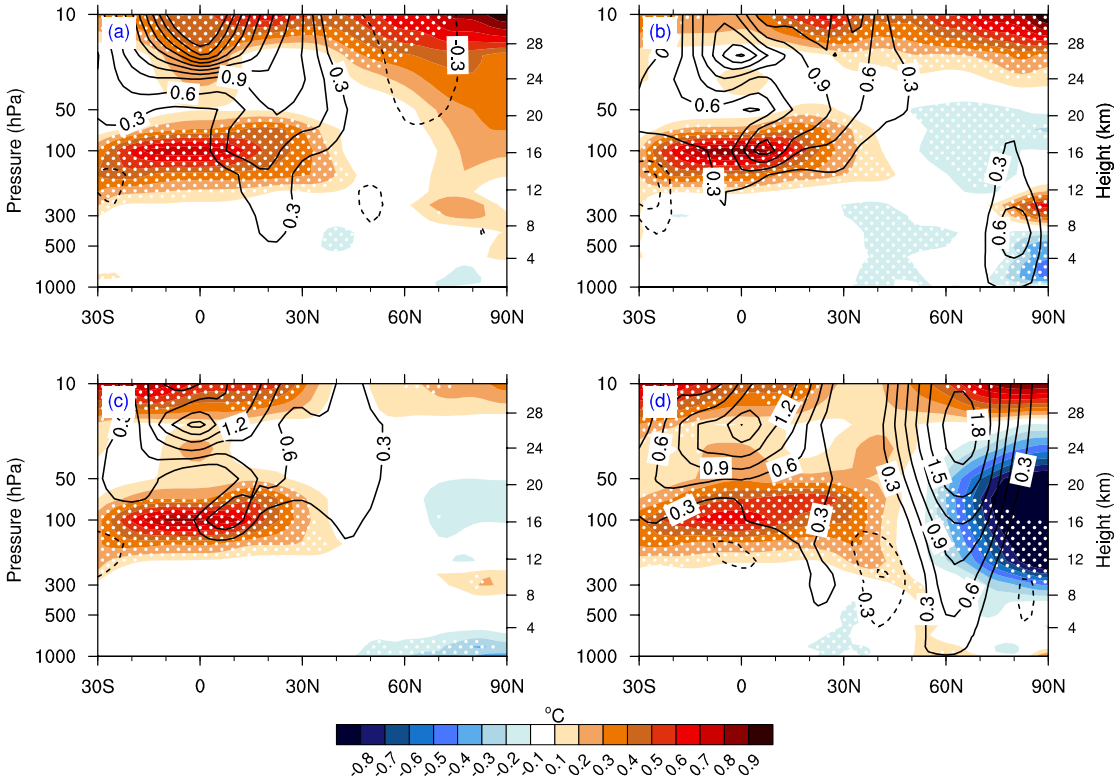

Figure 3. Persistence of anomalous signal in the atmosphere. Regression of zonally averaged zonal wind (contours) and air temperature (shading) in (**a**) Mar–May, (**b**) July–August, (**c**) September–November, and (**d**) December–February during 1964–2017 onto the normalized preceding annual mean of solar wind energy flux into the Earth's magnetosphere (E_{in}) index during 1963–2016. Stippled regions indicate that the temperature anomalies are significant at 90% confidence level from a two-tailed Student's *t* test.

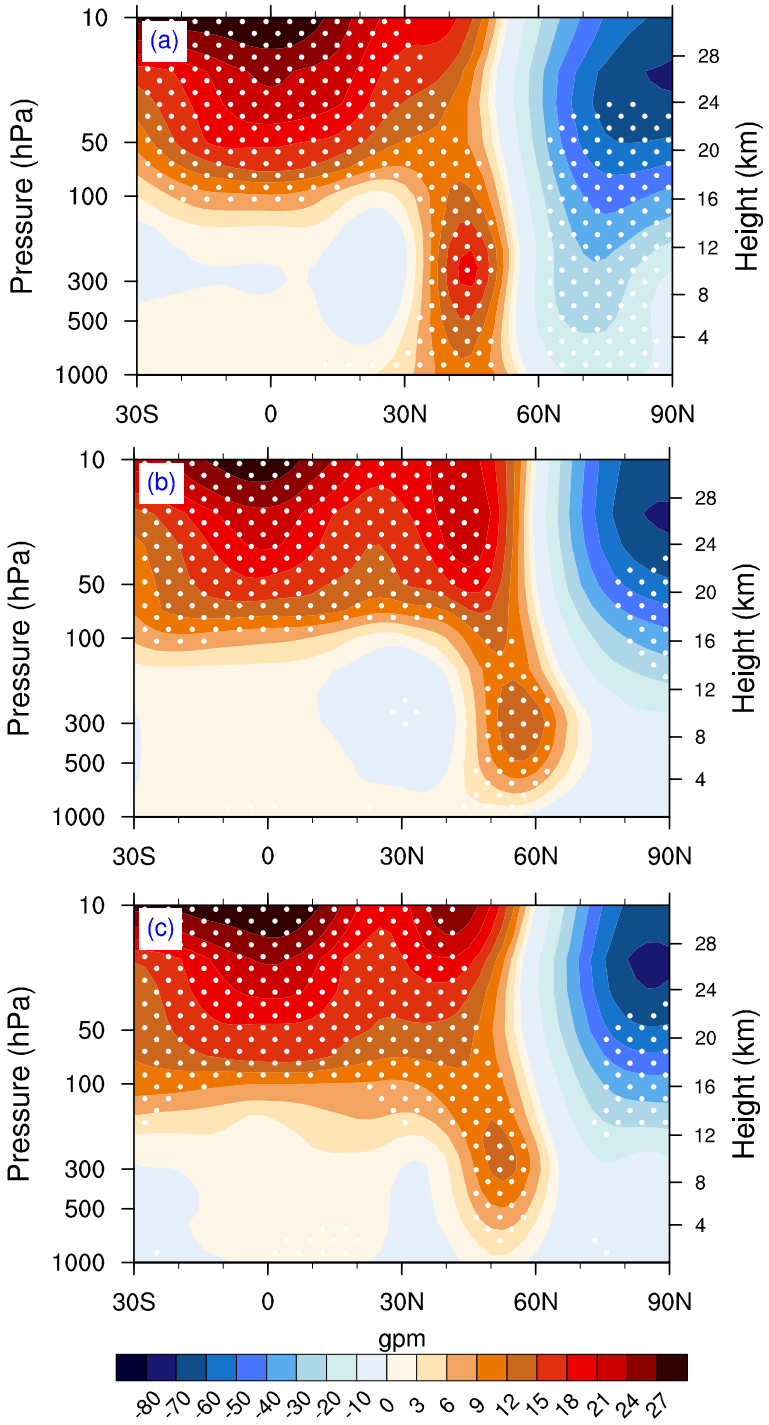

Figure 4. "Top-down" propagation of atmospheric anomalies. Vertical-horizontal cross section for geopotential height anomalies (shading) averaged along (a) 60°W–0°, (b) 90°E–150°E, and (c) 150°W–90°W during 1964–2017 winters onto the normalized preceding annual mean of solar wind energy flux into the Earth's magnetosphere (E_{in}) index during 1963–2016. Stippled regions indicate that the anomalies are significant at 90% confidence level from a two-tailed Student's *t* test.

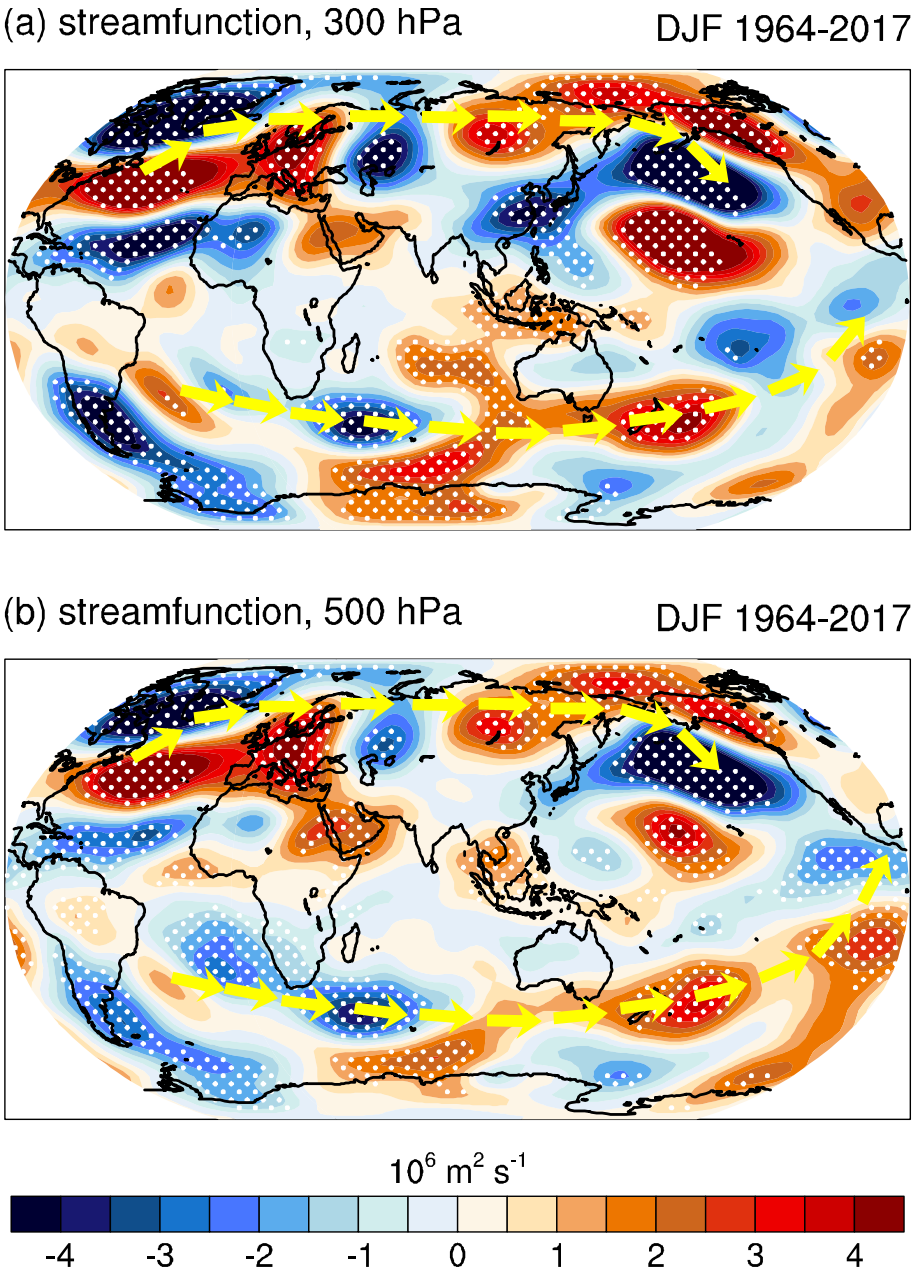

Figure 5. Schematic horizontal propagation of atmospheric teleconnection. Composite of streamfunction anomalies at (a) 300 hPa and (b) 500 hPa between the winters (1982, 1983, 1984, 1985, 1990, 1992, 1993, 2004) following higher-than-normal annual E_{in} and the ones (1964, 1965, 1966, 2008, 2009, 2010, 2011, 2012) following lower-than-normal annual E_{in} in 1963–2016. Stippled values are significant at the 90% confidence levels. The yellow arrows show schematically the main wave trains emanating for the North and South Atlantic.